Retention of nanocrystalline WN_x layers exposed to high-fluence deuterium plasmas

E. Vassallo [a, *], R. Caniello [a], G. Angella [b], D. Dellasega [a, c], G. Granucci [a], V. Mellera [a], D. Minelli [a], M. Pedroni [a], D. Ricci [a], V. Rigato [d], M. Passoni [a, c]

[a] CNR, Istituto di Fisica del Plasma "P. Caldirola", 20125 Milano, Italy
[b] CNR, Istituto per l'Energetica e le Interfasi, 20125 Milano, Italy
[c] Politecnico di Milano, Dipartimento di Energia, 20156 Milano, Italy
[d] INFN – Laboratori Nazionali di Legnaro, Legnaro, 35020 Padova, Italy

Received 30 April 2015
Received in revised form
2 September 2015
Accepted 3 September 2015
Available online 7 September 2015

1. Introduction

In next generation magnetic confinement fusion devices some plasma particles can escape from the magnetic confinement region and impact the surrounding wall. Such plasma-wall interactions critically affect tokamak operation in many ways. Plasma erosion determines the lifetime of plasma-facing components and creates a source of impurities, which can play a role in cooling and diluting the plasma [1]. Deposition of eroded impurities onto plasma-facing materials alters their surface composition and via co-deposition may lead to long-term accumulation of large in-vessel tritium inventories. Among the erosion mechanisms, the disruptions phenomena are a major concern for future tokamak reactors. High-velocity gas jet injection will be probably the technology used to mitigate disruptions [2]. Noble gas species and nitrogen are being studied on fusion device to investigate the physics of gas jet penetration and the ability of the gas jet impurities to convert plasma energy into radiation [3]. Although the use of N_2 gas to reduce the edge plasma temperature has recently been successfully applied in fusion devices such as ASDEX [4] and JET [5], questions remained about effects of N on the W plasma-facing components and ammonia production. In particular, the knowledge of the dependence of the hydrogen retention mechanisms in the W-N system is still limited and requires further research [6,7]. It is thus important to determine the parameters that govern the retention process as a function of W surface structure and composition.

The purpose of this study is to expose WN_x coatings with different properties (e.g. stoichiometry, crystallinity and N content) deposited using reactive Magnetron Sputtering (MS) to D plasmas with fluencies and energies that are expected in tokamak divertor areas ($\cong 10^{24}$ m^{-2}) and assess D retention level and distribution. The hydrogen retention in W exposed to low-energy deuterium plasma and ion beams has been studied [8–10] quite extensively by Thermal Desorption Spectroscopy (TDS) and Nuclear Reaction Analysis (NRA). The ERDA technique provides the depth profile of the deuterium concentration up to 200 nm in W using ^{7}Li ions [11] and up to 120 nm in WN_x samples using ^{4}He ions, furthermore the absolute concentrations for both isotopes, H and D, can be observed simultaneously.

* Corresponding author.
E-mail addresses: vassallo@ifp.cnr.it (E. Vassallo), caniello@ifp.cnr.it (R. Caniello), angella@ieni.cnr.it (G. Angella), david.dellasega@polimi.it (D. Dellasega), granucci@ifp.cnr.it (G. Granucci), mellera@ifp.cnr.it (V. Mellera), minelli@ifp.cnr.it (D. Minelli), pedroni@ifp.cnr.it (M. Pedroni), ricci@ifp.cnr.it (D. Ricci), valentino.rigato@lnl.infn.it (V. Rigato), matteo.passoni@polimi.it (M. Passoni).

2. Experimental details

2.1. WN_x coatings production

An RF plasma diode sputtering system [12] has been used to produce WN_x coatings as a function of seeding impurities (N). Coatings with thicknesses in the range of 1 μm were grown on Si substrates (1×1 cm^2, thickness $\cong$ 400 μm). The experimental apparatus consists of a parallel-plate, capacitive-coupled system, made up of a cylindrical stainless steel vacuum chamber with an asymmetric electrode configuration. A powered electrode is connected to an RF (13.56 MHz) power supply, coupled with an automatic impedance matching unit, while the other electrode, made up of stainless steel, is grounded. A 3-in diameter target of W (purity 99.9%) was placed on the powered electrode. Si substrates were placed on the ground electrode at 6.5 cm away from the powered electrode. No bias voltage was applied to the substrate holder. The substrates temperature was monitored by a thermocouple fixed directly on the substrate. Before the process, the substrates were cleaned with chemical etching solutions to remove surface contaminants. The process chamber was pumped to a base pressure below 1×10^{-5} Pa; high-purity gases were introduced into the vacuum chamber through a mass flow controller in order to establish the desired working pressure. Ar/N_2 mixtures were used as sputter gas. Total gas flow rate was fixed at 20 sccm. N_2 dilution was varied in the range 1–7 sccm. The RF power was fixed at 150 W (1500 V of DC self-bias voltage). The target was water cooled, and its temperature was kept below 20 °C during the coating process.

2.2. Coatings characterization

The morphological properties and physical structure of the films were investigated by Scanning Electron Microscopy (SEM). Measurements were performed using a ZEISS Supra System with an accelerating voltage of 5 kV. The structural properties studied by X-ray diffraction measurements were performed with a wide angle Siemens D-500 diffractometer (WAXD) equipped with a Siemens FK 60-10 2000W tube. The radiation was a Kα beam with wavelength $\lambda = 0.154$ nm. The operating voltage and current were 40 kV and 40 mA, respectively. The data were collected from 20 to 50 $2\theta^\circ$ at 0.02 $2\theta^\circ$ intervals by means of a silicon multi-cathode detector Vortex-EX (SII). The roughness was investigated by Atomic Force Microscopy (AFM in air by means of a Nano-RTM System (Pacific Nanotechnology, Santa Clara, CA, USA) operating in contact mode. The deposition rates were measured by a P15 surface profiler (KLATencor San Jose, CA) and by SEM.

2.3. D plasma exposure of coatings

WN_x samples were exposed to deuterium plasmas in the linear plasma device GYM [13]. It consists of a vacuum chamber (radius R = 0.125 m, length L = 2.11 m) mounted in a 0.13 T linear magnetic field (Fig. 1), in which a highly reproducible deuterium discharges are obtained and steadily sustained by microwaves (power up to 1.5 kW CW) in the electron cyclotron frequency range (2.45 GHz), injected perpendicularly to the magnetic field lines in O-mode polarization. The resonance at 0.0875 T is located in a single position close to the end of the vessel, opposite to the RF power launcher. The diagnostic setup is based on electrostatic probes spatially distributed for coherent structures detection (at present it is with 8 tips), on an imaging system using a fast framing camera and an image intensifier unit for direct visualization of the plasma structures (up to 200 kframes/sec). The plasma column has a radius of ~10 cm. The coatings have been exposed by a sample insertion system (Fig. 1) that consists of the sample head, the sample manipulator and the sample exchange chamber. The sample head is attached to the manipulator allowing the withdrawal of the sample from its exposure position to the sample exchange chamber. This sample exchange chamber can be isolated from the main vacuum chamber via a gate valve. The sample temperature was monitored by a thermocouple fixed directly on the sample holder. In all experiments, the measured temperature of the sample holder during the exposure process was in the range of 300–330 K.

All samples have been exposed to D_2 plasmas at a working pressure of 6.7×10^{-2} Pa with a total gas flow rate fixed at 30 sccm. The plasma state was driven by a 2.45 GHz RF generator at 1.5 kW of power. In this experimental condition, by mean of the Langmuir probe I–V characteristics, the following plasma parameters were found: plasma density $\cong 5.6 \times 10^{16}$ m^{-3}, plasma potential $\cong$ 12 V, electron temperature $\cong$ 4.4 eV. The ion flux Γ_i was calculated by the Bohm criterion [14,15] which yields

$$\Gamma_i = n_+ \exp(-0.5)\sqrt{\frac{kT_e}{m_+}}$$

where n_+ is the ion concentration, T_e is the electron temperature, m_+ is the mass of incident ion and k is the Boltzmann's constant. The ion flux was 5×10^{20} m^{-2} s^{-1} and with 1 h of plasma exposure the ion fluence was determined in $\cong 10^{24}$ m^{-2}.

2.4. Deuterium retention analysis

The near surface deuterium retention was determined with ex-situ ion beam analysis using Elastic Recoil Detection Analysis (ERDA) by the D(^{4}He,D)^{4}He reaction for near surface depth profile determination. In this technique, a monoenergetic He^+ beam with incident energy of 2.15 MeV impinges on the sample at grazing incidence (15° from the surface), and the energy spectrum of the forward-scattered deuterons and protons at 30° from the beam is obtained using a surface barrier detector. In this process, forward scattered He^+ are filtered out using a Mylar stopping foils ($\cong$ 12 μm). Parallel to the ERDA also the Elastic Backscattered particles were collected at 160° from the beam to determine the stoichiometry of the WN_xO_y surface layer.

3. Results and discussion

3.1. Deposition and characterization of WN_x coatings

Tungsten nitride coatings were prepared by diode sputtering in $Ar + N_2$ gas mixtures obtained by setting the total gas flow to 20 sccm at different Ar/N_2 flows. Based on our previous experience [16] in delamination mechanisms of thin films, in order to have mechanically stablecoatings, all coatings have been deposited in a bi-layer structure. The underlying layer is 800 nm thick and shows a partially porous and columnar morphology, the upper layer is 200 nm thick and exhibit a compact and columnar morphology. A typical SEM cross section is visible in Fig. 2 (bottom, left). This bi-layer structure was deposited by alternating high and low gas pressures (2 and 0.8 Pa), the topmost layer being deposited with the lowest pressure.

Surface morphology, roughness parameters, and grain size of WN_x films were analyzed using SEM. In Fig. 2 representative SEM images of WN_x film surfaces deposited at different nitrogen flow, from 0 to 7 sccm, are shown. The pure W film, deposited at 0 sccm, shows triangular crystalline grains of about 50 nm. These features are typical of W deposited by MS in Ar atmosphere [17]. The addition of a small amount of N_2 (0.5–1 sccm) induces a smoothing of the triangular morphology without affecting the grain size.

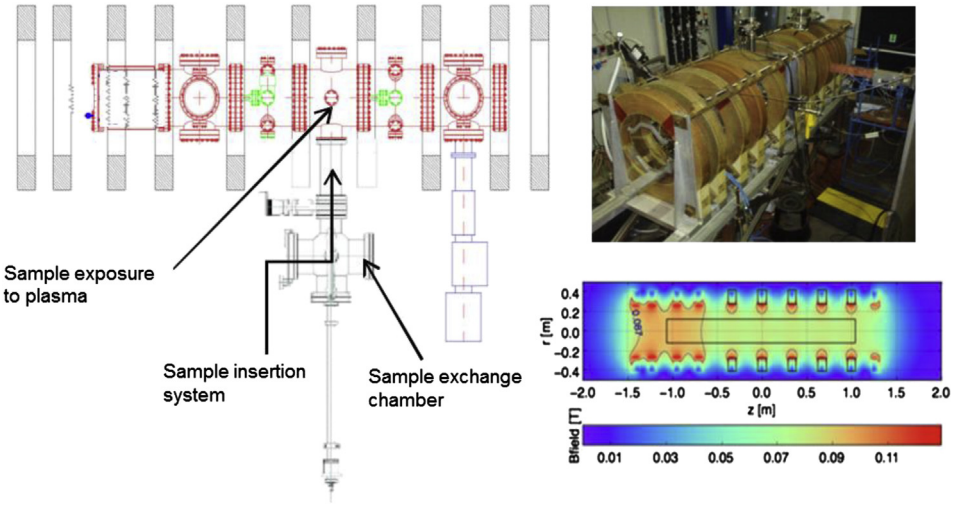

Fig. 1. GYM Linear plasma devices. Vacuum vessel, magnetic coil system and resonance layer.

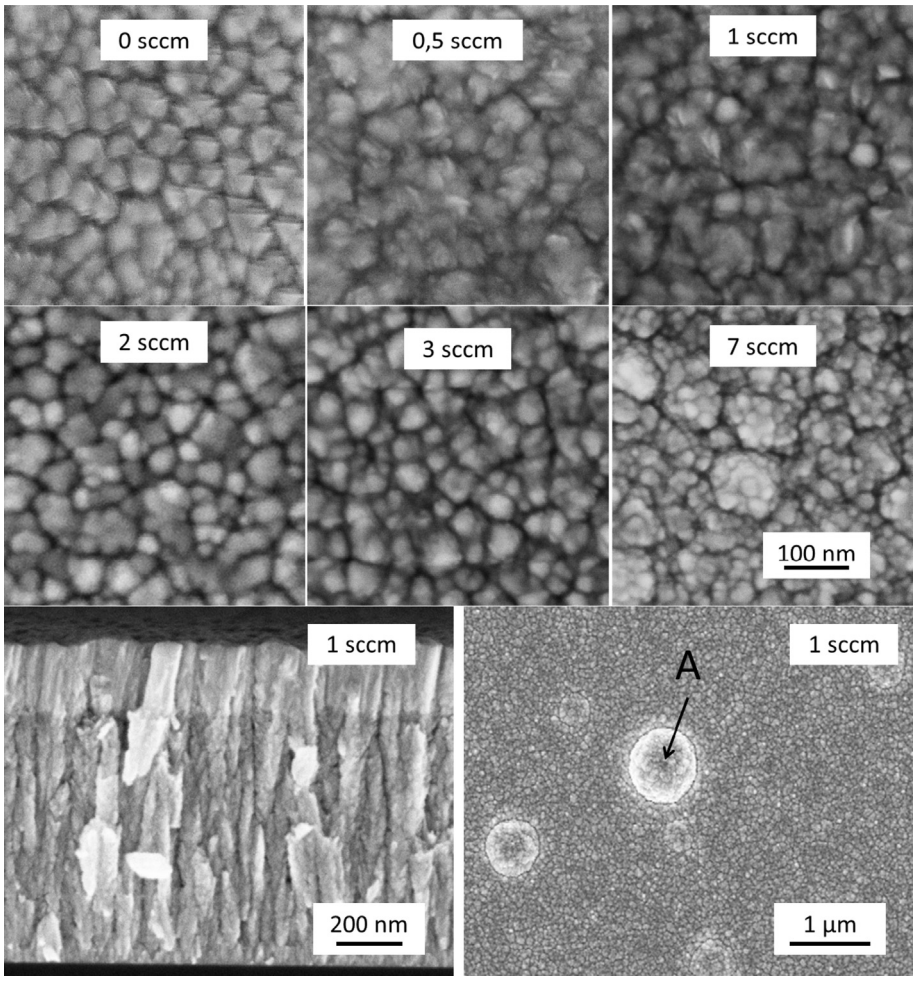

Fig. 2. (first and second row) Top view SEM images of a multilayer WN_x films produced at room temperature as a function of N_2 flow. (bottom, left) Cross-sectional SEM image at 0.5 sccm of N_2. (bottom, right) Top view SEM image (low magnification) at 1 sccm of N_2.

Raising N_2 amount (2–3 sccm) leads to a complete change of morphology, the growing film is made of smoother grains of 20–50 nm. A further increase of N_2 flow results in the formation of a more porous structure where small grains 20 nm are aggregated in bigger structures. It is worth noting that the films with a low N_2 flow ($\leq$1 sccm) show many micrometric cauliflower-like agglomerations in the surface (Fig. 2 bottom, right, marker A). The agglomerations decrease and disappear with the increase of N_2 flow.

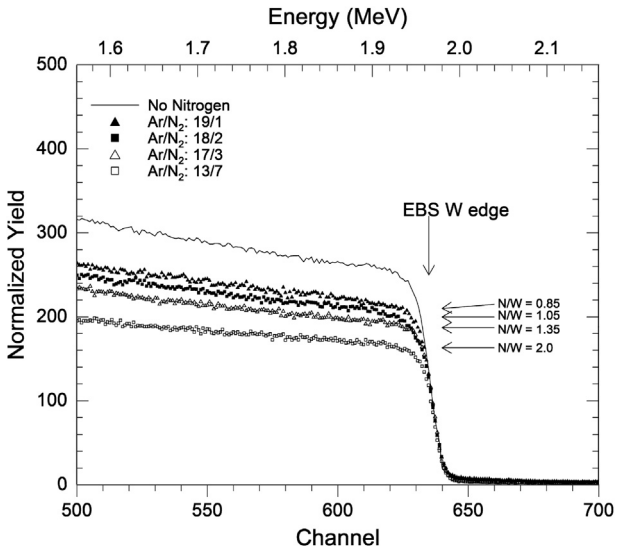

Fig. 3. W/N ratios in the WN_x coatings, as determined by RBS as a function of nitrogen flow. $E_\alpha = 2150$ KeV, $\Theta_{IN} = 75°$, $\Theta_{RBS} = 160°$.

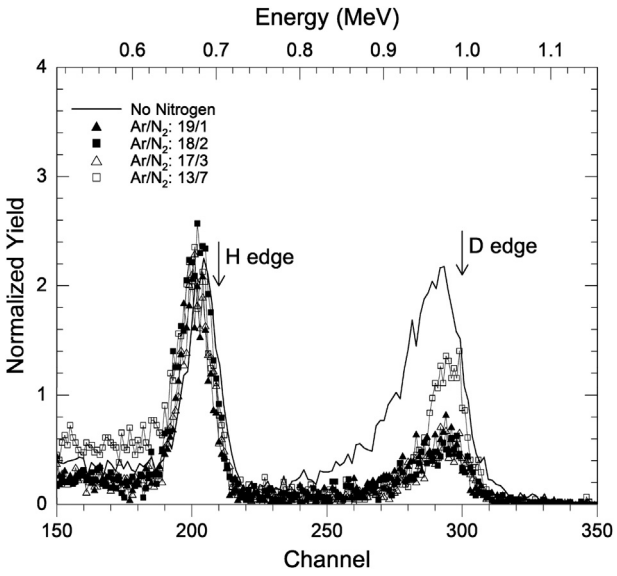

Fig. 5. ERDA spectra of deuterium and hydrogen in WN_x films obtained at increasing N_2 flow.

The roughness of the coatings has been investigated by AFM (measured on 2 μm scans) ranging the N_2 content. The RMS value of roughness exhibited a decrease from 6.4 to 2.1 nm following the morphology modifications found by SEM.

The progressive incorporation of nitrogen in tungsten was investigated by RBS analysis. In Fig. 3 the corresponding RBS spectra WN_x are shown. Nitrogen incorporation in the films increased as a function of N_2 flow: the N/W atomic ratio varied from about 0.85 to 2 for N_2 fluxes from 1 to 7 sccm. Oxygen contami-nation in the top layer was in the range 4–8 at%.

XRD analysis, displayed in Fig. 4, was used to determine the presence of crystalline phases in the WN_x films at varying nitrogen amount. The diffractogram "a" belongs to W coating deposited in absence of nitrogen flux. The film is composed of a mixture of α (bcc lattice) and β (A15 cubic lattice) phase of metallic W. In 2θ range from 34° to 42°, we observed the strongest (110) reflection of α-W and (200) reflection of β-W [18,19]. The reflections of metallic poly-crystalline tungsten disappear almost completely as a small amount of nitrogen (1/20) is injected in the gas mixture (see pattern "b"). In addition two small bands at 37° and 43° appear.

In the literature, in 2θ range from 36° to 48°, the nitride phases due to W and N could be mainly attributed to WN, W_3N_4 and W_2N [20–22]. Referring to the phase diagram of the W–N system [23], for the range of temperature (below 500 K) in our experiments, we assume that the WN nanocrystalline phase is formed. Raising N_2 flow at 2 sccm results in (see pattern "c") the increasing of reflections intensity. As the nitrogen amount increases (3 sccm), the peak position remains unchanged, but the intensity gradually decreases and becomes very weak for a N_2 flux of 7 sccm. This suggests that the nitrogen atoms are incorporated in the W matrix in a disordered structure decreasing the long-range crystallinity of the films and producing an amorphous WN_x coating.

The exposure of W surfaces to N plasmas, N ion fluxes and N discharges in Tokamak leads to the retention of N either in the elemental form or as a nitride [24,25]. The properties of WN_x

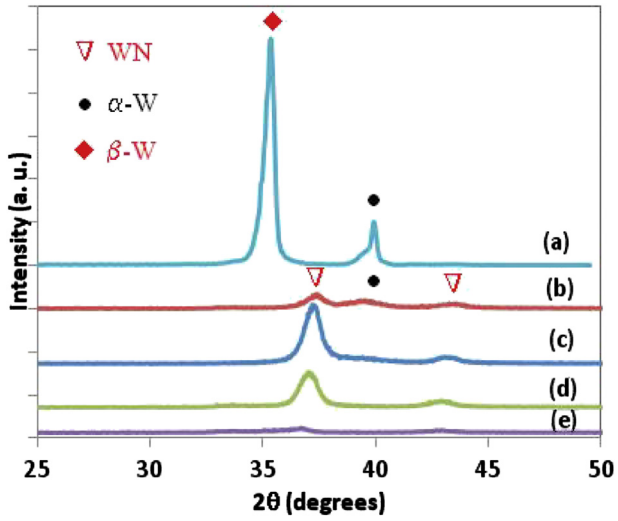

Fig. 4. XRD patterns of WN_x films as a function of N_2 flow: (a) $N_2 = 0$ sccm, (b) $N_2 = 1$ sccm, (c) $N_2 = 2$ sccm, (d) $N_2 = 3$ sccm, (e) $N_2 = 7$ sccm.

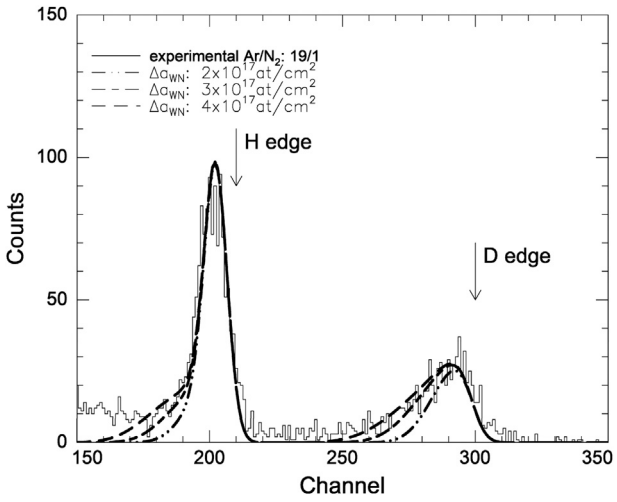

Fig. 6. ERD experimental spectrum taken at $\Theta_{IN} = 75°$, $\Theta_{ERD} = 30°$, $E_z = 2150$ KeV using 12 μm Mylar absorber foil. $I_{Beam} = 20–25$ nA. Simulations of different thicknesses of surface deuterated layer are shown.

Table 1
Surface D content as measured by ERDA. Data refer to deuterium in the maximum analyzable depth.

N_2 flux (sccm)	N_2 partial pressure (10^{-2} Pa)	N/W ratio in the coating	Coating structure	Deuterium content $\times 10^{19}$ at/m^2
0 (no nitrogen)	0	0	α -W + β -W	9.5
1	4	0.85	α -W + WN	2.0
2	8	1.05	Cryst.-WN	1.7
3	12	1.35	Cryst.-WN	1.6
7	28	2	Amorph.-WN	2.9

coatings produced using Ar/N_2 mixture are similar to those obtained after exposure to N plasmas. In fact considering the WN stoichiometry detected using XRD, (W/N ratio equal to 1) and the N/W ratio determined using RBS (0.85–2) it is possible to state that if a N_2 flow higher than 3 sccm is used nitrogen is stored in the film both in the elemental form and as a compound.

3.2. Exposure in GyM and deuterium retention

WN_x samples were exposed to deuterium plasmas in the linear plasma device GyM. After exposure no evidence of surface modification like blisters or bubbles was present. Deuterium interactions with the WN_x coatings were analyzed with ERDA using ^{4}He ions. The resulting spectra are shown in Fig. 5. Comparing the collected spectra and simulations made using SIMNRA code [26], using published cross section data [27,28], it is possible to calculate the surface penetration depth and content of the retained deuterium.

The ERDA experimental spectra show that the deuterium is mainly accumulated in the near-surface layers of the WN_x samples. The maximum analyzable depth by ERDA (i.e. in the spectral region between the Deuterium and the Hydrogen surface peaks shown in Fig. 5) in WN_x is about 120 nm. The near surface D detection limit in our experimental conditions is of order of 0.1 at %. The ERD spectra reported in Fig. 5 show that the D profile is rapidly decreasing below the experimental detection limit after few tens of nanometers from surface even in the pure W sputtered films. We cannot rule out the possibility of a tail extending beyond the maximum analyzable depth, characterized by a concentration below our ERDA detection limit. The thickness of the near surface deuterated layer can be studied through a simulation as shown in Fig. 6. The simu-lations show that the region interested by most deuterium uptake is about 3–4 $\times$ 10^{17} at/cm^2 of WN_x (corresponding to a maximum of about 60 nm). Deuterium penetration depth is of the same order of magnitude of deuterium implanted in crystalline WN_x coatings prepared by MS [6].

The measured surface D content (Table 1) is strongly affected by the structure and composition of the WN_x coatings. In absence of nitrogen, D retention in pure W coatings (9.5×10^{19} D/m^2) is similar to that found in other D plasma exposure experiments [29]. Nanocrystalline WN_x coatings seem to lead to a decrease of D retention compared with the case of pure W ($\approx 2 \times 10^{19}$ D/m^2). For the WN_x coating with high N content in the amorphous phase an increase in the amount of retained D ($\approx 3 \times 10^{19}$ D/m^2), with respect to nanocrystalline WN, is observed. Retention properties of crystalline WN_x coating or N implanted W depending on energy of the impinging D ions and exposure temperature were studied [7,29]. In these studies at low temperature (300 K) the amount of retained D in WN_x matrix seems to be substantially equivalent to that of pure W. On the other side, it has been observed that nanostructured or amorphous coatings may behave quite differently compared to the corresponding crystalline ones. In W coatings the presence of an amorphous or nanocrystalline structure induces higher D retention levels compared with microcrystalline bulk W [30]. The same conclusions are reported for bulk tungsten self-damaged by W implantation [31]. In addition, it is reported that the presence of an amorphous W compound (e.g. W oxide) in some cases lowers the amount of retained deuterium compared to W coating [32].

4. Conclusions

WN_x layers have been deposited in an RF plasma system and exposed to high fluence (~10^{24} m^{-2}) deuterium plasma in a linear device (GYM) at room temperature. ERDA analyses show that the deuterium is mostly retained in the surface layer (few tens of nanometers). As determined by SEM, the morphology of WN_x compounds is very similar, and it does not appear to be decisive for D retention. On the other hand, XRD measurements and RBS analysis show substantial differences of the coatings structure as a function of nitrogen stoichiometry. Results on the D retention show that nitrogen in the process of tungsten redeposition in tokamak could play a very important role. Incorporation of nitrogen in tungsten decreases the D retention. All samples produced with nitrogen dilution show a level of D retention lower than the acceptable limit for tritium (T) operation in ITER (i.e. 2.5×10^{20} T/m^2 $\approx$ 1 mg of T/m^2).

Acknowledgments

This work, partially supported by the European Communities under the contract of Association EURATOM/ENEACNR, was carried out within the framework of EFDA (Task WP13-IPH-A03-P1-02/ENEA_CNR). The views and opinions expressed here do not necessarily reflect those of the European Commission.

References

[1] Y. Ueda, T. Tanabe, V. Philipps, et al., J. Nucl. Mater 220–222 (1995) 240.
[2] R. Granetz, D.G. Whyte, V.A. Izzo, T. Biewer, M.L. Reinke, J. Terry, A. Bader, M. Bakhtiari, T. Jernigan, G. Wurden, Nucl. Fusion 46 (2006) 1001–1008.
[3] Y. Tanga, Z.Y. Chen, Y.H. Luo, Y.B. Dong, D.W. Huang, W. Jin, R.H. Tong, W. Yan, W.G. Ba, G. Zhuang, Phys. Lett. A 379 (2015) 1043–1047.
[4] A. Kallenbach, R. Dux, J.C. Fuchs, et al., Plasma Phys. Control. Fusion 52 (2010) 055002.
[5] M. Oberkofler, D. Douai, S. Brezinsek, J.W. Coenen, T. Dittmar, A. Drenik, S.G. Romanelli, E. Joffrin, K. McCormick, M. Brix, G. Calabro, M. Clever, C. Giroud, U. Kruezi, K. Lawson, Ch Linsmeier, A. Martin Rojo, A. Meigs, S. Marsen, R. Neu, M. Reinelt, et al., J. Nucl. Mater. vol. 438 (Supplement) (July 2013) S258–S261.
[6] L. Gao, W. Jacob, T. Schwarz-Selinger, A. Manhard, et al., J. Nucl. Mater. 451 (2014) 352–355.
[7] L. Gao, W. Jacob, P. Wang, U. von Toussaint, A. Manhard, Phys. Scr T159 (2014) 014023.
[8] A.A. Haasz, J.W. Davis, M. Poon, R.G. Macaulay-Newcombe, J. Nucl. Mater 258–263 (1998) 889.
[9] O.V. Ogorodnikova, B. Tyburska, V.Kh Alimov, K. Ertl, J. Nucl. Mater 415 (2011) S661.
[10] A. Manhard, K. Schmid, M. Balden, W. Jacob, J. Nucl. Mater 415 (2011) S632.
[11] S. Markelj, O.V. Ogorodnikova, P. Pelicon, T. Schwarz-Selinger, I. Čadež, Appl. Surf. Sci. 282 (2013) 478–486.
[12] H.R. Koenig, L.I. Maissel, IBM J. Res. Dev. 14 (1970) 168.
[13] G. Granucci, D. Ricci, et al., in: Proc.36th EPS Conf. on Pl. Phys, ECA 33E, Sofia, Bulgaria, 2009. P-4.148.
[14] D. Bohm, in: A. Guthrie, R.K. Wakerling (Eds.), The Characteristics of Electrical Discharges in Magnetic Fields, McGraw-Hill, New York, 1949.

[15] H. Kersten, R.J.M.M. Snijkers, J. Schulze, G.M.W. Kroesen, H. Deutsch, et al., Appl. Phys. Lett. 64 (1994) 1496.
[16] E. Vassallo, R. Caniello, A. Cremona, G. Croci, D. Dellasega, G. Gorini, G. Grosso, E. Miorin, M. Passoni, M. Tardocchi, Surf. Coatings Technol. 214 (2013) 59–62.
[17] E. Vassallo, R. Caniello, M. Canetti, D. Dellasega, M. Passoni, Thin Solid Films 558 (2014) 189–193.
[18] S.M. Rossnagel, I.C. Noyan, J.C. Cabral, J. Vac. Sci. Technol. B 20 (5) (2002) 2047.
[19] N.M.G. Parreira, N.J.M. Carvalho, F. Vaz, A. Calveiro, Surf. Coat. Technol. 200 (2006) 6511–6516.
[20] M. Bereznai, Z. Tòth, A.P. Caricato, M. Fernandez, A. Luches, G. Majni, P. Mengucci, P.M. Nagy, A. Juhasz, L. Nanai, Thin Solid Films 473 (2005) 16–23.
[21] Jae Hyung Kim, Kyung Lim Kim, Appl. Catal. A General 181 (1999) 103–111.
[22] Tai-Nan Lin, Sheng Han, Ko-Wei Weng, Chin-Tan Lee, Thin Solid Films 529 (2013) 333–337.
[23] K. Schmid, A. Manhard, Ch Linsmeier, A. Wiltner, T. Schwarz-Selinger, W. Jacob, S. Mändl, Nucl. Fusion 50 (2010) 025006.
[24] M. Rubel, V. Philipps, L. Marot, P. Petersson, A. Pospieszczyk, B. Schweer, et al., J. Nucl. Mater. 415 (2011) S223–S226.
[25] L. Laguardia, R. Caniello, A. Cremona, D. Dellasega, et al., J. Nucl. Mater. (2015), http://dx.doi.org/10.1016/j.jnucmat.2014.12.087.
[26] M. Mayer, Proceedings of the 15th International Conference on the Application of Accelerators in Research and Industry, in: J.L. Duggan, I.L. Morgan (Eds.), American Institute of Physics Conference Proceedings 475, 1999, p. 541.
[27] A.J. Kellock, J.E.E. Baglin, Nucl. Instr. Meth Phys. Res B79 (1993) 493.
[28] V. Quillet, F. Abel, M. Schott, et al., Nucl. Instr. Meth B83 (1993) 47.
[29] O.V. Ogorodnikova, K. Sugiyama, T. Schwarz-Selinger, T. Dürbeck, M. Balden, J. Nucl. Mater. 419 (1) (12/2011) 194–200.
[30] M.H.J. 't Hoen, et al., J. Nucl. Mater. (2015), http://dx.doi.org/10.1016/j.jnucmat.2014.11.025.
[31] S. Markelj, et al., J. Nucl. Mater. 438 (2013) S1027–S1031.
[32] A Pezzoli, D. Dellasega, V. Russo, A Gallo, ZeijImans P A Emmichoven, M. Passoni, doi:10.1016/j.jnucmat.2014.11.035.